INTERNATIONAL JOURNAL OF HYDROGEN ENERGY 35 (2010) 5786–5792

Available at www.sciencedirect.com

ScienceDirect

journal homepage: www.elsevier.com/locate/he

Control of a grid-assisted wind-powered hydrogen production system

José G. García Clúa [a,*], *Hernán De Battista* [a], *Ricardo J. Mantz* [b]

[a] CONICET, LEICI, Facultad de Ingeniería, Universidad Nacional de La Plata, C.C. 91 (1900) La Plata, Argentina
[b] CICpBA, LEICI, Facultad de Ingeniería, Universidad Nacional de La Plata, C.C. 91 (1900) La Plata, Argentina

ARTICLE INFO

Article history:
Received 2 December 2009
Received in revised form
22 December 2009
Accepted 18 February 2010
Available online 20 March 2010

Keywords:
Hydrogen production
Electrolysis
Wind energy
Control
Sliding mode control

ABSTRACT

This paper deals with the control of a H_2 production system supplied by wind power and assisted by the grid. The system architecture consists of a pitch-controlled wind turbine coupled through a diode rectifier to an alkaline electrolyzer, which in turn is connected to the electric grid through a fully-controlled bidirectional electronic converter. A control strategy for the electronic converter is proposed to regulate the electrolyzer current at its rated value. Thus, H_2 production efficiency is optimized despite wind power and temperature variability. Control design is based on sliding mode techniques, which are particularly appropriate to control fast switching devices and exhibit strong robustness properties. Additionally, in high wind speeds, a pitch control loop is activated to limit the wind power capture below admissible values.

1. Introduction

Hydrogen production from renewable energies is a highly topical subject. Indeed, several studies in the field have been reported in the literature during the last years [1–5]. Among the current options for clean H_2 production, wind-powered water electrolysis ranks high in terms of technical and economical feasibility, having a great potential to be the route towards the H_2 economy [6–12]. The wind resource is characterized by short-term and seasonal variability whereas water electrolyzers have not been conceived to operate under variable input conditions. Then, special care must be taken when coupling electrolyzers to wind turbines. In particular, the following requirements must be considered for their proper operation [13–19]:

1. H_2 production efficiency and purity of produced gases increase with current. Therefore, electrolyzers should be operated above a minimum current I_E min, which is typically around 25–40% of rated.
2. H_2 production rate is proportional to charge transfer flow, *i.e.* to electric current. Then, electrolyzers should be operated at rated current I_E^N when maximum H_2 production is desired.
3. Electrolyzer operation should not be interrupted in order to protect the electrodes from corrosion and to avoid dangerous diffusion of gases.
4. Fast current gradients should be avoided since they increase internal wear, impurities and energy losses.

In this work, a wind-H_2 system with grid assistance is considered. The advantage of this concept is that the grid can serve to smooth wind power fluctuations and to guarantee the safe and proper operation of the electrolyzer. Several operation policies can be followed. Here, the priority is to produce H_2 at maximum rate and quality. With this aim, a control

* *Corresponding author*. Tel./fax: +54 221 4259306.
E-mail address: jose.garciaclua@ing.unlp.edu.ar (J.G. García Clúa).

doi:10.1016/j.ijhydene.2010.02.098

system is designed to regulate the electrolyzer current at rated value despite wind turbulence. In low winds, the electrolyzer is complementarily supplied by the wind turbine and the grid, whereas in high winds the grid filters the wind power fluctuations that cannot be smoothed by the pitch control mechanism. The main contribution of the paper lies in the control design. A sliding mode (SM) controller is developed that provides excellent regulation features over the operating region despite wind power variations. The controller performance is validated by simulation using realistic wind speed profiles and equipments data.

2. System architecture

Fig. 1 sketches the system configuration. A pitch-controller wind turbine drives a permanent magnet synchronous generator (PMSG) connected to the electrolyzer by means of a diode rectifier. On the other side, a bidirectional power converter couples the wind-H_2 system to the grid. Mathematical models of the subsystems are presented in successive paragraphs, which can then be integrated into a dynamical model of the whole system.

2.1. Alkaline electrolyzer

The electrical behavior of an electrolyzer is usually described by the aggregated model of individual electrolytic cells. The theoretical voltage between electrodes necessary to initiate the reaction that dissociates water is called reversible cell voltage U_{rev}. The output voltage of the cell U_{cell} is always higher than U_{rev}. The difference between them, called polarization, is primarily due to electrical resistance losses and to kinetic over-voltages known as activation and concentration potentials [20]. The characteristic curve of an alkaline electrolyzer comprising n cells can be approximated by the empiric formula [21]:

$$u_E = nU_{cell} = n\left[U_{rev} + \frac{r_e}{A}i_E + s_e \ln\left(\frac{t_e}{A}i_E + 1\right)\right] \quad (1)$$

where u_E and i_E are the electrolyzer voltage and current, respectively, A is the electrode area, and r_e, s_e and t_e are coefficients that change with the electrolyte temperature T_E. Coefficient r_e models the ohmic losses, whereas s_e and t_e are kinetic over-voltage coefficients.

Fig. 2 shows the current–voltage characteristic of a 60 kW alkaline electrolyzer at two different operating temperatures.

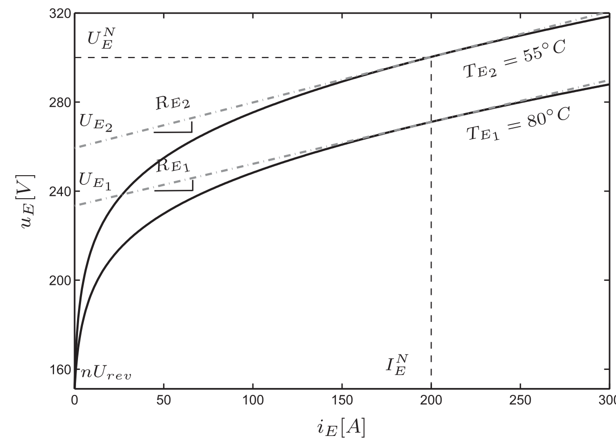

Fig. 2 – Typical current–voltage curves of an electrolyzer.

It can be observed that there is an almost linear behavior in the high current region where ohmic losses predominate over kinetic over-voltage potentials [19]. Therefore, a circuital representation consisting in a voltage source (U_E) with output resistance (R_E) is valid in this region [22]. Both U_E and R_E vary with T_E.

2.2. Wind turbine

The power P_T captured by a wind rotor of radius R facing an airflow of speed υ and density ρ is

$$P_T = \frac{1}{2}\rho\pi R^2 c_P(\lambda, \beta)\upsilon^3 \quad (2)$$

where c_P describes the turbine aerodynamics as function of the pitch angle β and the tip-speed-ratio $\lambda = R\Omega_T/\upsilon$, with Ω_T being the rotational speed at the hub. The dynamics of the wind turbine is mainly governed by

$$J\Omega_T \frac{d\Omega_T}{dt} = P_T(\Omega_T, \beta, \upsilon) - T_G\Omega_G \quad (3)$$

where Ω_G and T_G are the speed and reaction torque of the PMSG, and J is the inertia of the drive-train referred to the left-side of the gearbox, which is aimed at matching turbine and generator speeds ($\Omega_G = k_{gb}\Omega_T$). Variable-pitch wind turbines give the opportunity to control the aerodynamic torque and limit the power capture by rotating their blades. The pitch actuator, together with its control mechanism, will be addressed at the end of Section 3.

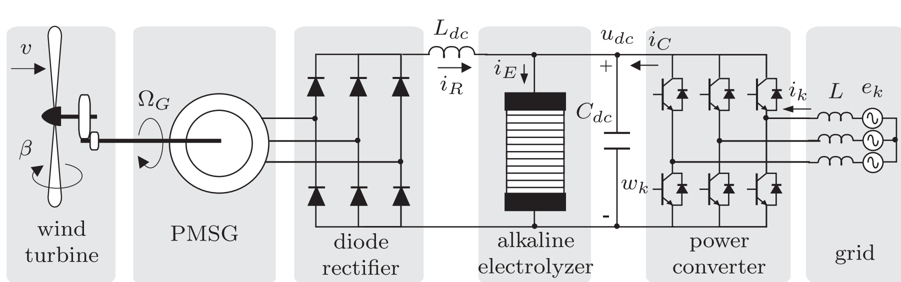

Fig. 1 – Block diagram of the grid-assisted wind-H_2 system.

2.3. Generator – diode rectifier

From stator terminals, the PMSG can be modeled as a star-connected 3-phase sinusoidal voltage source u_G in series with synchronous inductance L_G. The peak voltage value is $\widehat{U}_G = p\Phi\Omega_G$ where p is the number of magnetic pole pairs and Φ is the concatenated magnetic flux. The stator currents are rectified by the 3-phase diode rectifier, and then smoothed by inductor L_{dc} and DC-bus capacitor C_{dc}. Assuming that the rectifier is loaded by a current source, the DC-component $\overline{u}_R$ of voltage at rectifier terminals can be modeled as a voltage source of open-circuit voltage U_R with series resistance R_R:

$$\overline{u}_R = U_R - R_R\bar{i}_R = \left(\frac{3\sqrt{3}}{\pi}\widehat{U}_G\right) - \left(\frac{3p}{\pi}L_G\Omega_G\right)\bar{i}_R \tag{4}$$

where $\bar{i}_R$ is the DC-component of the output current i_R, and U_R and R_R can be derived with little effort. The voltage drop $R_R\bar{i}_R$ puts in evidence the diode currents overlapping that can be attributed to L_G [23].

Since electrical dynamics is much faster than the mechanical one (3), a static model of the electrical behavior suffices. Neglecting losses in electromechanical conversion, mechanical (input) and electrical (output) powers are equal:

$$T_G\Omega_G = u_R i_R. \tag{5}$$

2.4. Bidirectional electronic converter – grid

The electronic circuit used to handle the electrical power exchanged with the grid is a 3-phase voltage-source power converter [23]. Each leg k of the converter comprises two bidirectional switches. At each time, only one of these switches is in conduction. The state of conduction of each converter leg can therefore be represented by a switching signal w_k, which takes the value 1 when the upper switch is on and -1 when the lower switch is on.

The grid is modeled as a perfect 3-phase sinusoidal system $e_{\{k\}}$, with peak phase voltages E and angular frequency ω, in series with a phase inductance L. The 3-phase grid currents are called $i_{\{k\}}$. Usually, it is much convenient to represent signals in a rotating quadrature reference frame d–q, rather than on a static one $k = 1, 2, 3$. In the d–q representation, sinusoidal signals take constant values. The transformation between both representation frames is

$$A_{dq}^{k} = \frac{2}{3}\begin{bmatrix} \cos(\theta) & \cos\left(\theta - \frac{2\pi}{3}\right) & \cos\left(\theta + \frac{2\pi}{3}\right) \\ -\sin(\theta) & -\sin\left(\theta - \frac{2\pi}{3}\right) & -\sin\left(\theta + \frac{2\pi}{3}\right) \end{bmatrix} \tag{6}$$

where $\theta = \omega t$. That is $e_{\{dq\}} = A_{dq}^{k} e_{\{k\}}$, $i_{\{dq\}} = A_{dq}^{k} i_{\{k\}}$, $w_{\{dq\}} = A_{dq}^{k} w_{\{k\}}$. The d-axis is aligned so that $e_d = E$ and $e_q = 0$. Then, the instantaneous active and reactive power flowing through the grid lines are

$$P = \frac{3}{2}Ei_d, \quad Q = \frac{3}{2}Ei_q. \tag{7}$$

The dynamic behavior of grid currents is described by

$$\begin{cases} L\dfrac{di_d}{dt} = e_d + \omega L i_q - \dfrac{u_{dc}}{2}w_d \\ L\dfrac{di_q}{dt} = e_q - \omega L i_d - \dfrac{u_{dc}}{2}w_q \end{cases} \tag{8}$$

where u_{dc} is the DC-side voltage source. The DC-side converter current i_C is

$$i_C = \frac{3}{4}\left(w_d i_d + w_q i_q\right). \tag{9}$$

In Fig. 1, the wind-driven generator, electrolyzer and power converter are connected to a common DC-bus, *i.e.* $\overline{u}_R = u_E = u_{dc}$. So, the DC-bus dynamics is

$$C_{dc}\frac{du_{dc}}{dt} = i_R + i_C - i_E. \tag{10}$$

3. Control design

The overall system dynamics present three separate time scales. On the one hand, the system exhibits very fast grid current dynamics, which is due to the low inductance value of grid inductors L. On the other hand, the dynamics of the mechanical subsystem is very low because of the large inertia. Finally, the DC-bus dynamics is designed much faster than the mechanical one, but much slower than the grid current dynamics. This motivates the control scheme shown in Fig. 3 that consists of three feedback loops having different bandwidth. One control loop is aimed at controlling the rectifier current i_R in order to limit wind power capture. The other control loops are cascaded, the inner control loop is intended to regulate the grid currents by a suitable converter switching pattern, whereas the outer loop regulates the electrolyzer current by using grid currents as control inputs. These control schemes are described below in more detail.

3.1. Grid currents control loop

The objective of this feedback loop is to regulate grid currents $i_{\{dq\}}$ at given values $i^{*}_{\{dq\}}$. These controlled variables exhibit the relative-degree-one condition, that is the control inputs $w_{\{dq\}}$ explicitly appear in the time derivative of $i_{\{dq\}}$. Then, according to variable structure system theory, the controlled variables can be forced to reach their desired values in finite time by means of a suitable switching action. That is, the so-called sliding surface defined by

$$S_{\{dq\}} = \begin{bmatrix} i_d^{*} - i_d & i_q^{*} - i_q \end{bmatrix}^T = 0 \tag{11}$$

can be reached in finite time. Once the surface is reached, the current dynamics can be constrained to this surface by a fast switching action. This mode of operation of variable structure systems is called sliding regime. The necessary and sufficient condition for SM existence on surface $S_{\{dq\}} = 0$ is that, locally,

$$\lim_{S_{\{dq\}} \to 0} S^T_{\{dq\}}\dot{S}_{\{dq\}} < 0. \tag{12}$$

This condition can be interpreted geometrically as the necessity that the state trajectory points towards the surface from its both sides. From (12) and (8), conditions on $w_{\{dq\}}$ from both sides of the surface can be derived. However, since the switching signal was originally defined in the stationary reference frame, with admissible values $w_k = \pm 1$, it is convenient to transform the surface coordinate function $S_{\{dq\}}$ to the stationary reference frame and then command the converter switches with

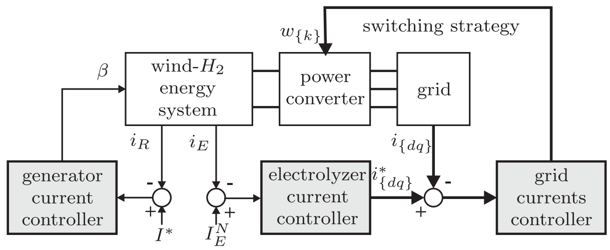

Fig. 3 – Control scheme.

$$w_{\{k\}} = -\text{sign}\left(\left(A_{dq}^{k}\right)^{T} S_{\{dq\}}\right), \quad k = 1, 2, 3. \tag{13}$$

From the grid current dynamics (8) and the switching control signal (13), the SM existence condition (12) can be rewritten as follows:

$$\left(\frac{u_{dc}}{3}\right)^{2} > \left(L\omega i_d^*\right)^2 + \left(E + L\omega i_q^*\right)^2 \tag{14}$$

which means that DC-bus voltage must be kept above a given value for proper operation of the power converter.

From (7), it is clear that i_d is responsible for the active power transmission whereas i_q is associated to reactive power. Here, we set $i_q^* = 0$ so that the power converter does not exchange reactive power with the grid. On the other hand, when current i_d is regulated at i_d^*, the active power equals the DC-side converter power, that is $u_{dc} i_C = (3/2)E i_d^*$. This power balance condition will be exploited in the next subsection to control the electrolyzer current using i_d^* as control input.

3.2. *Electrolyzer current control loop*

This outer control loop is aimed at regulating the electrolyzer current at its rated value despite wind power fluctuations as well as variations in electrolyte temperature. A nonlinear proportional-integral controller is proposed, which guarantees stability of the controlled system at every feasible operating point. It takes advantage that the inner control loop previously described effectively regulates i_d at i_d^* so that, from the DC-bus side, the electronic converter can be seen as a current source of value $i_C = 3E i_d^*/(2u_{dc})$.

The dynamic response of the control loop can be derived from the DC-bus circuital scheme depicted in Fig. 4. The leftmost arm of the circuit represents the electrical behavior of the wind-driven generator (see Eq. (4)). Recall that both U_R and R_R change with rotational speed. Diode D means that current can flow only from generator to DC-bus. That is, when wind speed is very low, more precisely is not high enough to sustain a generator voltage $U_R > u_{dc}$, then the generator does not supply current. The electrolyzer is also modeled as a voltage source U_E in series with an output resistance R_E (see Fig. 2).

From this equivalent circuit, the DC-bus dynamics (10) can be rewritten as follows

$$C_{dc}\frac{du_{dc}}{dt} = \frac{U_R - u_{dc}}{R_R} - \frac{u_{dc} - U_E}{R_E} + \frac{3E i_d^*}{2u_{dc}} \tag{15}$$

where the first term in the right-hand side becomes zero if $U_R < u_{dc}$. This DC-bus dynamics is expanded with an integral state x_q to eliminate steady state errors:

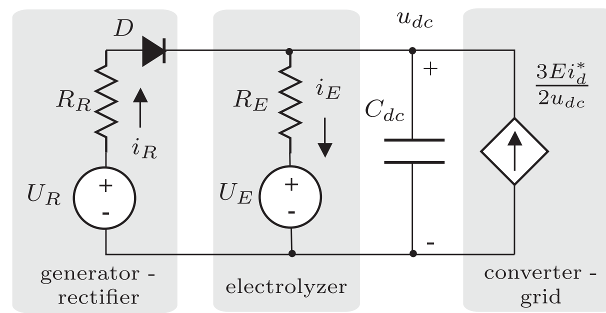

Fig. 4 – Circuital scheme of the DC-bus.

$$\dot{x}_q = I_E^N - i_E. \tag{16}$$

Now, the following nonlinear proportional-integral feedback is proposed:

$$i_d^* = u_{dc}\left(k_1 u_{dc} + k_2 x_q + k_3\right) \tag{17}$$

such that the expanded DC-bus dynamics becomes linear, taking the form $dx/dt = Ax + b$ with $x = [u_{dc} \quad x_q]^T$,

$$A = \begin{bmatrix} \frac{3k_1E}{2C_{dc}} - \frac{1}{RC_{dc}} & \frac{3k_2E}{2C_{dc}} \\ -\frac{1}{R_E} & 0 \end{bmatrix}, b = \begin{bmatrix} \frac{U_R}{R_R} + \frac{U_E}{R_E} + \frac{3k_3E}{2C_{dc}} \\ I_E^N + \frac{U_E}{R_E} \end{bmatrix} \tag{18}$$

where $R = R_E||R_R$ if $U_R > u_{dc}$, otherwise $R = R_E$. Also, the term U_R/R_R should be removed from the first entry in b when $U_R < u_{dc}$.

To guarantee stability of the equilibrium point $x_0 = -A^{-1}b$, the eigenvalues $\lambda_{1,2}$ of matrix A must have negative real part. This occurs whenever $k_1 < 2/(3ER)$, $k_2 > 0$. Besides, to avoid interaction with the inner control loop, the outer loop dynamics should be designed much slower than the inner one, i.e. $|\lambda_{1,2}| \ll \lambda^{max} = R/L$. A conservative gain tuning that guarantees stability for any feasible equilibrium point is

$$\begin{cases} k_1^* = \frac{C_{dc}}{3E}\left[\left(\frac{1}{R^{min}} + \frac{1}{R^{max}}\right)\frac{1}{C_{dc}} - \frac{\lambda^{max}}{2}\right]. \\ k_2^* = R_E^{min} C_{dc} \left(\lambda^{max}\right)^2/(48E) \end{cases} \tag{19}$$

On the other hand, gain k_3 does not affect stability but the steady state value of the integral state. So, it must be designed to avoid integrator saturation.

3.3. *Generator current control*

A third control loop is designed to limit the wind power production. The controlled variable is the wind-driven generator current whereas the control input is the pitch angle. By pitching the blades, the wind turbine power coefficient c_P and therefore the wind power capture can be controlled. The pitch servo can be modeled as a slow first-order dynamical system with time constant τ_β, with

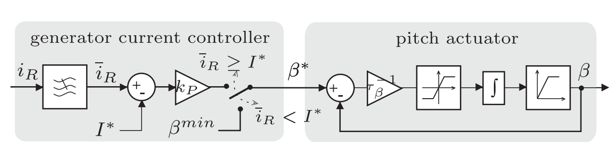

Fig. 5 – Diagram of pitch actuator and generator current controller.

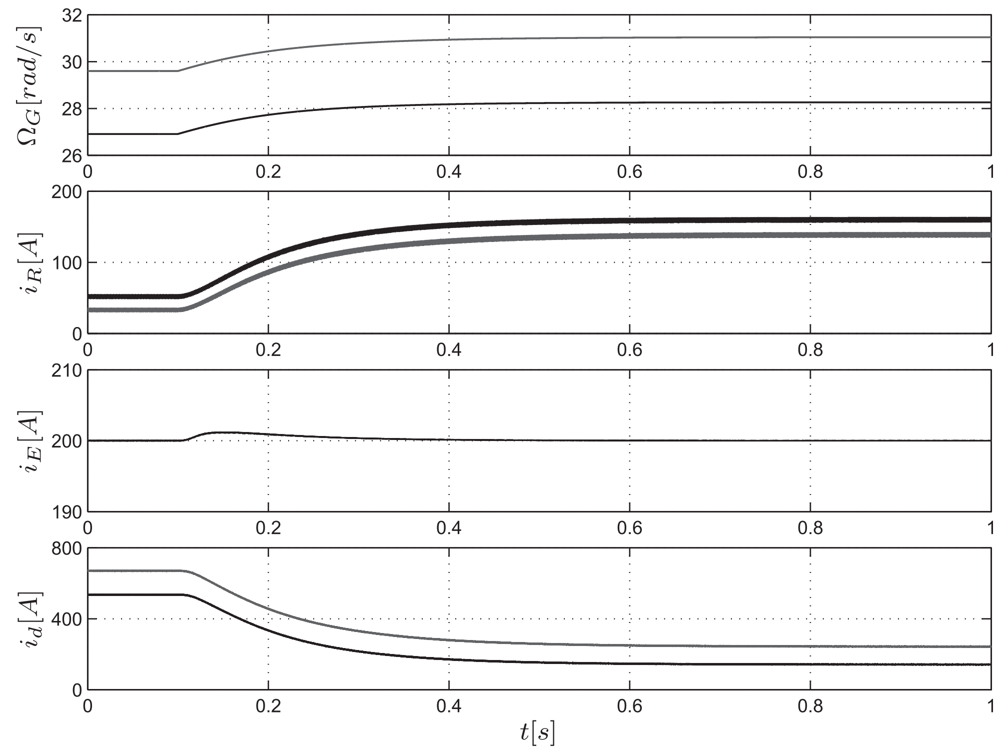

Fig. 6 – Controlled system response to a wind speed step from 6 to 8 m/s for two different T_E: 80° (black) and 55° (gray).

amplitude and rate saturation [24]. A block diagram of the pitch servo dynamics and generator current controller can be observed in Fig. 5.

The controller becomes active when the generator current tries to exceed a prescribed value I^*. For instance, I^* may be the rated current of the generator I_R^N when it is desired to inject as much wind power as possible to the grid, or the rated current of the electrolyzer I_E^N when injecting wind power to the grid is not desired. On the other hand, when generator current is below I^*, the controller remains inactive and the pitch angle is maintained at its minimum value $\beta = \beta^{\min}$.

As can be seen in the figure, a proportional controller is used in this paper. Gain k_P is designed to limit over-current to an admissible value ΔI max, *i.e.* $k_P = (\beta^{\max} - \beta^{\min})/\Delta I^{\max}$.

The dynamics of the control loop can be derived from (3)–(5) and Fig. 5:

$$\begin{cases} J\Omega_T \frac{d\Omega_T}{dt} = P_T(\Omega_T, \beta, v) - \bar{i}_R(\Omega_T, u_{dc})u_{dc} \\ \tau_\beta \frac{d\beta}{dt} = k_P(\bar{i}_R(\Omega_T, u_{dc}) - I^*) - \beta \end{cases} \quad (20)$$

where u_{dc} is regulated by the electrolyzer current controller. Stability of the pitch control loop can be verified by linearizing (20) and checking eigenvalues position.

4. Numerical results

In this section, the theoretical results are corroborated using numerical simulation. The overall system is modeled in Matlab environment using the Sim Power Systems toolbox. The system consists of a variable-pitch 100 kW wind turbine, a synchronous generator of the same power and rated speed $\Omega_G^N = 350$ rpm, a 60 kW alkaline electrolyzer ($I_E^N = 200$ A) and a 60 kW power converter.

The first simulation run is aimed at showing the regulation features of the two-loop electrolyzer current controller. As it is common practice in control engineering, we have analyzed the step response of the controlled system. In fact, a sudden step in the wind speed from 6 to 8 m/s was simulated for two values of electrolyte temperature, and the response is plotted in Fig. 6. The increasing wind power accelerates the generator until a higher operating speed is reached. The current supplied by the generator increases three times. The in-phase converter current i_d is adjusted accordingly by the SM controller so that the electrolyzer current rapidly converges to its rated value. The quadrature current i_q remains at zero. Despite the wind speed perturbation (20% of its rated value $v^N = 10.5$ m/s) and different electrolyte temperature, the electrolyzer current deviates only 0.5% from its rated value. In real world, such an abrupt wind speed change will not occur, and electrolyzer current will be even less perturbed.

The second simulation run shows the response to a realistic wind speed profile ranging from low to high wind speeds. The results are displayed in Fig. 7. Two cases were considered. In the first one, the wind turbine captures as much power as possible to supply the electrolyzer and inject power to the grid. The pitch angle is adjusted above rated wind speed in order to limit the wind turbine power to its rated value ($I^* = I_R^N$). In the second case it is supposed that it is not desired to inject wind power to the grid, so the reference for the pitch controller is $I^* = I_E^N$. It is observed that the electrolyzer current is much smoother than the generator one thanks to the grid assistance and the two-loop

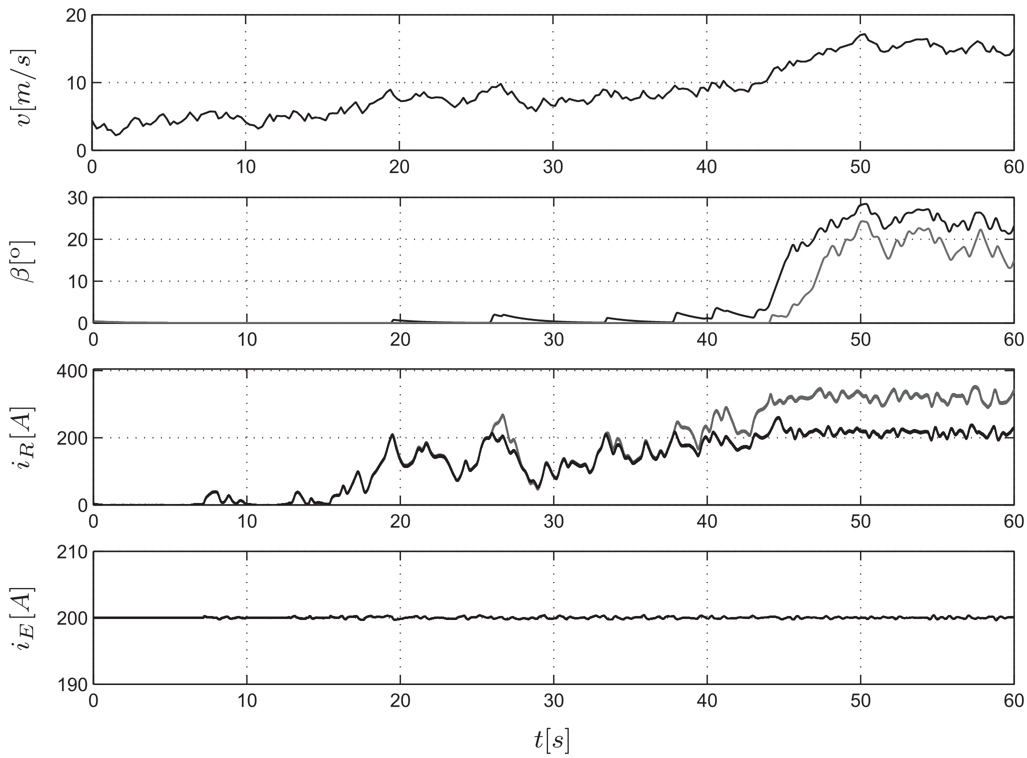

Fig. 7 – Controlled system response to realistic wind speed profile with generator current regulation at I_E^N (black) and I_R^N (gray).

current controller. It can be interpreted as that the grid filters the wind power fluctuations. In both cases, the electrolyzer current is regulated at its rated value with an error lower than 0.5%. Thus, hydrogen is produced at the maximum rate of 12.5 $Nm^3\,h^{-1}$.

5. Conclusions

This paper addresses the control of a grid-assisted wind-H_2 energy system. The primary control objective is to operate the electrolyzer under nominal conditions. This objective is fulfilled by means of a cascaded controller of the power converter that couples the system to the grid. The proposed SM approach provides stability and robustness against wind power fluctuations and electrolyte temperature uncertainties. Additionally, a pitch controller was developed to actively control the wind power injected to the grid under high wind speed conditions. Simulation results using a realistic wind speed profile corroborate the attractive features of the system architecture and control scheme. Grid assistance together with the proposed control method allows improving H_2 production efficiency and quality. Storage devices and other renewable resources can be easily incorporated thanks to the modularity of system architecture and control.

Acknowledgments

This work was funded by ANPCyT (PICT 2007-00535), CONICET (PIP 112-200801-01052/09), CICpBA and UNLP (11/I127) of Argentina.

REFERENCES

[1] Dunn S. Hydrogen futures: toward a sustainable energy system. Int J Hydrogen Energy 2002;27(3):235–64.

[2] Santarelli M, Calì M, Macagno S. Design and analysis of stand-alone hydrogen energy systems with different renewable sources. Int J Hydrogen Energy 2004;29(15): 1571–86.

[3] IEA. Prospects for hydrogen and fuel cells, tech. report. Int Energy Agency. Available from: http://www.iea.org; 2005.

[4] Afgan N, Veziroglu A, Carvalho M. Multi-criteria evaluation of hydrogen system options. Int J Hydrogen Energy 2007; 32(15):3183–93.

[5] Contreras A, Guirado R, Veziroglu T. Design and simulation of the power control system of a plant for the generation of hydrogen via electrolysis, using photovoltaic solar energy. Int J Hydrogen Energy 2007;32(18):4635–40.

[6] Elam C, Padró C, Sandrock G, Luzzi A, Lindblad P, Fjermestad Hagene E. Realizing the hydrogen future: the International Energy Agency's efforts to advance hydrogen energy technologies. Int J Hydrogen Energy 2003;28(6):601–7.

[7] Sherif S, Barbir F, Veziroglu T. Wind energy and the hydrogen economy – review of the technology. Sol Energy 2005;78:647–60.

[8] Bockris J, Veziroglu T. Estimates of the price of hydrogen as a medium for wind and solar sources. Int J Hydrogen Energy 2007;32(12):1605–10.

[9] Greiner C, Korpås M, Holen A. A Norwegian case study on the production of hydrogen from wind power. Int J Hydrogen Energy 2007;32(10–11):1500–7.

[10] Troncoso E, Newborougha M. Implementation and control of electrolysers to achieve high penetrations of renewable power. Int J Hydrogen Energy 2007;32(13):2253–68.

[11] Moriarty P, Honnery D. Intermittent renewable energy: the only future source of hydrogen? Int J Hydrogen Energy 2007; 32(12):1616–24.

[12] Segura I, Pérez-Navarro A, Sánchez C, Ibáñez F, Payá J, Bernal E. Technical requirements for economical viability of electricity generation in stabilized wind parks. Int J Hydrogen Energy 2007;32(16):3811–9.
[13] Dutton A, Bleijs J, Dienhart H, Falchetta M, Hug W, Prischich D, et al. Experience in the design, sizing, economics, and implementation of autonomous wind-powered hydrogen production systems. Int J Hydrogen Energy 2000;25(8):705–22.
[14] Miland H. Operational experience and control strategies for a stand-alone power system based on renewable energy hydrogen. Phd thesis, Norwegian Univ of Sci & Tech, Trondheim; 2005.
[15] De Battista H, Mantz R, Garelli F. Power conditioning for a wind-hydrogen energy system. J Power Sources 2006;155: 478–86.
[16] Gandía L, Oroz R, Ursúa A, Sanchis P, Diéguez P. Renewable hydrogen production: performance of an alkaline water electrolyzer working under emulated wind conditions. Energy Fuels 2007;21:1699–706.
[17] Korpås M, Greiner C. Opportunities for hydrogen production in connection with wind power in weak grids. Renew Energy 2008;33(6):1199–208.
[18] García Clúa J, Mantz R, De Battista H. Hybrid control of a photovoltaic-hydrogen energy system. Int J Hydrogen Energy 2008;33:3455–9.
[19] Ursúa A, Marroyo L, Gubía E, Gandía L, Diéguez P, Sanchisa P. Influence of the power supply on the energy efficiency of an alkaline water electrolyser. Int J Hydrogen Energy 2009;34(8): 3221–33.
[20] Korpås M. Distributed energy systems with wind power and energy storage. Phd thesis, Norwegian Univ of Sci & Tech; 2004.
[21] Ulleberg Ø. Modeling of advanced alkaline electrolyzers: a system simulation approach. Int J Hydrogen Energy 2003; 28(1):21–33.
[22] Fingersh L. Optimized hydrogen and electricity generation from wind, tech. report TP-500-34364. NREL; 2003.
[23] Bose B. Power electronics and AC drives. Prentice-Hall; 1986.
[24] Bianchi F, De Battista H, Mantz R. Wind turbine control systems. Springer; 2007.